Spectral analysis of craters on (101955) Bennu

J.D.P. Deshapriya, M.A. Barucci, E.B. Bierhaus, S. Fornasier, P.H. Hasselmann, F. Merlin, B.E. Clark, A. Praet, M. Fulchignoni, A.A. Simon, et al.

Spectral analysis of craters on (101955) Bennu

J. D. P. Deshapriya [a], M. A. Barucci [a], E. B. Bierhaus [b], S. Fornasier [a,c], P. H. Hasselmann [a], F. Merlin [a], B. E. Clark [d], A. Praet [a], M. Fulchignoni [a], A. A. Simon [e], V. E. Hamilton [f], E. A. Cloutis [g], C. Lantz [h], X. D. Zou [i], J.-Y. Li [i], D. C. Reuter [e], J. R. Brucato [j], G. Poggiali [j,k], R. T. Daly [ℓ], D. Trang [m], S. Ferrone [d], D. N. DellaGiustina [n], D. S. Lauretta [n]

[a] *LESIA, Observatoire de Paris, Université PSL, CNRS, Université de Paris, Sorbonne Université, 5 place Jules Janssen, 92195 Meudon, France*

[b] *Lockheed Martin Space, Littleton, CO, USA*

[c] *Institut Universitaire de France (IUF), 1 rue Descartes, 75231 PARIS CEDEX 05, France*

[d] *Department of Physics, Ithaca College, Ithaca, NY 14850, United States*

[e] *NASA Goddard Space Flight Center, Greenbelt, MD 20771, USA*

[f] *Southwest Research Institute, Boulder, CO, USA.*

[g] *Department of Geography, University of Winnipeg, Winnipeg, Manitoba, Canada*

[h] *Institut d'Astrophysique Spatiale, CNRS/Université Paris Saclay, Orsay, France*

[i] *Planetary Science Institute, Tucson, AZ, USA*

[j] *INAF Astrophysical Observatory of Arcetri, Florence, Italy*

[k] *Department of Physics and Astronomy, University of Florence, Firenze, Italy*

[ℓ] *Johns Hopkins University Applied Physics Laboratory, Laurel, MD, USA*

[m] *Hawai'i Institute of Geophysics and Planetology, University of Hawai'i, Honolulu, HI, United States*

[n] *Lunar and Planetary Laboratory, University of Arizona, Tucson, AZ, USA*

Number of pages: 31
Number of tables: 1
Number of figures: 11

Preprint submitted to Icarus *30 November 2020*

Proposed Running Head:
TBD

Please send Editorial Correspondence to:

J D Prasanna Deshapriya
Bureau 34, Bâtiment 17
LESIA-Observatoire de Paris
5 Place Jules Janssen
92195 Meudon Cedex
FRANCE

Tel. : +33-145077666
Mobile : +33-781790489
Email : prasanna.deshapriya@obspm.fr

ABSTRACT

Using data acquired by the OSIRIS-REx (Origins, Spectral Interpretation, Resource Identification, and Security–Regolith Explorer) mission, we investigate spectral properties of craters on the near-Earth asteroid (101955) Bennu. We compare Bennu's craters with its global average by means of four spectral parameters: (a) minimum position of the band at 2.7 μm, (b) depth of the hydrated phyllosilicate absorption band at 2.7 μm, (c) normalized spectral slope from 0.55 to 2.0 μm, and (d) reflectance factor at 0.55 μm. We examine 45 craters using spectral data obtained under various observing conditions. For 20 craters, we find a shortward shift of the 2.7-μm band minimum relative to the global 2.7-μm band minimum, which we attribute to the presence of relatively fresh (less space-weathered) material excavated from the sub-surface by crater-forming impacts. For three craters, we find an anti-correlation between spectral slopes and reflectance factor for a series of spectra acquired during a specific scan, where we observe that spectra become redder and darker towards the center of the crater. We attribute this to the presence of fine-particulate regolith. Localized spectral heterogeneities are apparent inside a prominent equatorial crater on Bennu, which is one of the asteroid's oldest geological features. We propose that such local spectral heterogeneities could be used as a tracer of mass movement on Bennu. We show that younger craters are redder, brighter, and have deeper 2.7-μm bands. Comparing global average spectral values of Bennu and crater frequency distributions as a function of the chosen spectral parameters, we find that craters evolve to assume the global average spectral properties of Bennu. A positive correlation identified between the reflectance factor and 2.7-μm band depth suggests that brighter craters tend to be more hydrated. Finally, we put into context, the results from the Small Carry-on Impactor experiment by the Hayabusa2 spacecraft, which created an artificial crater on the near-Earth asteroid (162173) Ryugu.

Keywords: spectroscopy; NEAs; space missions; planetary science; craters;

1 Introduction

The study of impact craters has furthered the understanding of the solar system in many aspects (Melosh (1989)). Craters form on planetary surfaces due to an almost instantaneous release of energy during an impact event. They are present on many solar system bodies at different scales and are often a proxy for understanding the geo-physical nature of the body in question (Strom et al. (2005), Fassett (2016), Robbins et al. (2018)). Whether primary, secondary (Bierhaus et al. (2018)), or sesquinary, craters can represent extensive geological modifications on planetary bodies. The preservation of craters depends on the relative rates of geological processes that erase them and the flux of impactors that create them. For example, while Earth and the Moon are exposed to approximately the same impactor flux (other than differences due to gravitational focusing and Earth's atmosphere), their crater abundances are different because of the different rates of geological activity.

Distributions of craters are used to estimate surface ages and understand the history of planetary surfaces. In addition, because crater-forming impacts lead to excavation and spreading of ejecta, craters offer natural laboratories to investigate sub-surface material. The compositional and physical characterization of sub-surface material, which should be fresher (less space-weathered) than the constantly exposed surface, is important for quantitative analysis of weathering processes and evolutionary paths of planetary bodies. Comprehensive spectral studies are becoming widely possible for asteroids and dwarf planets, expanding our knowledge about cratering and their evolutionary processes in varying gravity regimes (Hirata et al. (2020), Galiano et al. (2019), Longobardo et al. (2019), Cho et al. (2019), Arakawa et al. (2017)). In this work, we focus on the spectral properties of some of the craters present on the near-Earth asteroid (NEA) (101955) Bennu, as explored by NASA's Origins, Spectral Interpretation, Resource Identification, and Security–Regolith Explorer (OSIRIS-REx) space mission (Lauretta et al. (2017)).

The prime objective of the OSIRIS-REx mission is to globally characterize Bennu and return a sample of pristine carbonaceous material from it. Bennu is spectrally classified as a B-type (DeMeo et al. (2009)), a sub-group of the C-complex asteroids, characterized by a blue spectrum (Clark et al. (2011)). It is spectrally associated with organic-rich hydrated carbonaceous chondrites, in particular, the aqueously altered CMs and CIs (Hamilton et al. (2019)), tracing back to primitive material from the formation of the solar system (Lauretta et al. (2015)). Data collected by the OSIRIS-REx spacecraft in proximity to Bennu reach scales of 3.8 mm/px for the OSIRIS-REx Camera Suite (OCAMS; Rizk et al. (2018)) and about 1 m/footprint for the OSIRIS-REx Visible and InfraRed Spectrometer (OVIRS; Reuter et al. (2018)). Further, lidar scans by the OSIRIS-REx Laser Altimeter (OLA; Daly et al. (2017)) form the basis of

digital terrain models (DTMs) and high-resolution shape models (Barnouin et al. (2019), Barnouin et al. (2020), Daly et al. (2020)). As such, the topography of Bennu has been characterized sufficiently to identify impact craters on its surface (Walsh et al. (2019), Bierhaus et al., in preparation).

The distribution of impact craters on Bennu has implications for its dynamic lifetime as an NEA and on the evolutionary path that it took since its departure from the main asteroid belt (Walsh et al. (2019), Bottke et al. (2020)). Preliminary analysis by Walsh et al. (2019) showed that a large crater located on the equatorial ridge of Bennu predates (0.1 to 1 billion years) Bennu's expected lifetime (10 million years) in near-Earth space by more than an order of magnitude, meaning that it traces back to Bennu's time in the main asteroid belt. A layer of infilling material about 6 m thick on the southern side of this crater is attributed to mass movement (Walsh et al. (2019), Jawin et al. (2020)).

Spectral data from the spacecraft encounter with Bennu have shown a ubiquitous 2.7-μm absorption band centred at 2.74±0.01 μm, indicative of Mg/Fe-rich **phyllosilicates on Bennu** (Hamilton et al. (2019), Simon et al. (2020)). The spacecraft data verified Bennu's global visible-to-near-infrared blue spectrum and low albedo (DellaGiustina et al. (2019), Hamilton et al. (2019)). However, Bennu has local variations in albedo and color (DellaGiustina et al. (2020)). Given this spectral background of Bennu, this study uses OVIRS data to probe four spectral parameters that offer insight into the spectral properties of craters on Bennu. On the basis of these four parameters, we determine **if and** how the spectral behavior of craters on Bennu is distinct from the global average.

2 Data & Methods

2.1 Selection criteria for identifying craters

After analysis of the spatial coverage of OVIRS spectral data against the catalogue of craters on Bennu (Bierhaus et al. (2019)), we selected 45 craters for study. The availability of spectral data influenced the selection of craters. **Bierhaus et al. (2019) report 598 craters whose dimensions correspond down to the smallest crater included in this study. Therefore, our analysis of 45 craters is comparable to about 7.5% of identified craters on Bennu that are equal or larger than the smallest crater we studied.**

Fig. 1 depicts the locations of the craters included in this study, overlain on an

equirectangularly projected global mosaic of Bennu (Bennett et al. (2020)). Characteristics of these craters are recorded in Table 1 in Appendix A. The locations and diameters of the craters are sourced from Bierhaus et al., (in preparation).

The frequency of analyzed craters as a function of diameter is visualized in Fig. 2. As specified in Table 1, the OVIRS data used in this work span several different observational phases of the OSIRIS-REx mission. When more than one data set was available for a selected crater, we selected the data set with the best spatial coverage of the crater.

We used high-resolution shape models and DTMs (Barnouin et al. (2019), Barnouin et al. (2020), Daly et al. (2020)) produced from OLA data to visualize craters in three dimensions and compute parameters of interest such as dynamic height and local computed using rotation state and mass distribution of Bennu (Thomas (1993), Scheeres (2012), Scheeres et al. (2019), Scheeres et al. (2020)). These shape models also facilitated the photometric correction of the data by enabling the derivation of facet-based incidence (i), emission (e), and phase angles (α). We used the Small Body Mapping Tool (Ernst et al. (2018)) for visualizations of these data along with python library vtkplotter (Musy et al. (2019)). We used the spiceypy python package (Annex et al. (2020)), which is a python wrapper for the SPICE Toolkit (Acton (1996), Acton et al. (2018)), for facet-based calculations.

2.2 Spectral data

The OVIRS point spectrometer has a circular aperture with a field-of-view of 4 mrad and operates in the spectral range of 0.4 to 4.3 μm. OVIRS data are acquired using five filter segments, and a spectrum is reconstructed according to the steps detailed in Reuter et al. (2018). The data are calibrated according to the procedure described in Simon et al. (2018), which is based on the data acquired during the OSIRIS-REx Earth flyby and was updated after arrival at Bennu (Simon et al. (2020)). The ground calibration pipeline converts the raw data (counts per second) to spectral radiance units ($\mathrm{Wcm^{-2}\ \mu m^{-1} sr^{-1}}$) and then to the unitless quantity radiance factor (RADF), upon the removal of the thermal emission. Finally, RADF is divided by the solar incident flux at the given heliocentric distance of the observation (Simon et al. (2020)). The data are then converted to photometrically corrected reflectance factor (REFF) at the geometry of i=30°,e=0°,α=30°, according to Zou et al. (2020). This geometry was chosen for this study because it facilitates comparison with spectral data from meteorites and clay minerals.

Most of the spectral data used in this study come from the Equatorial Station

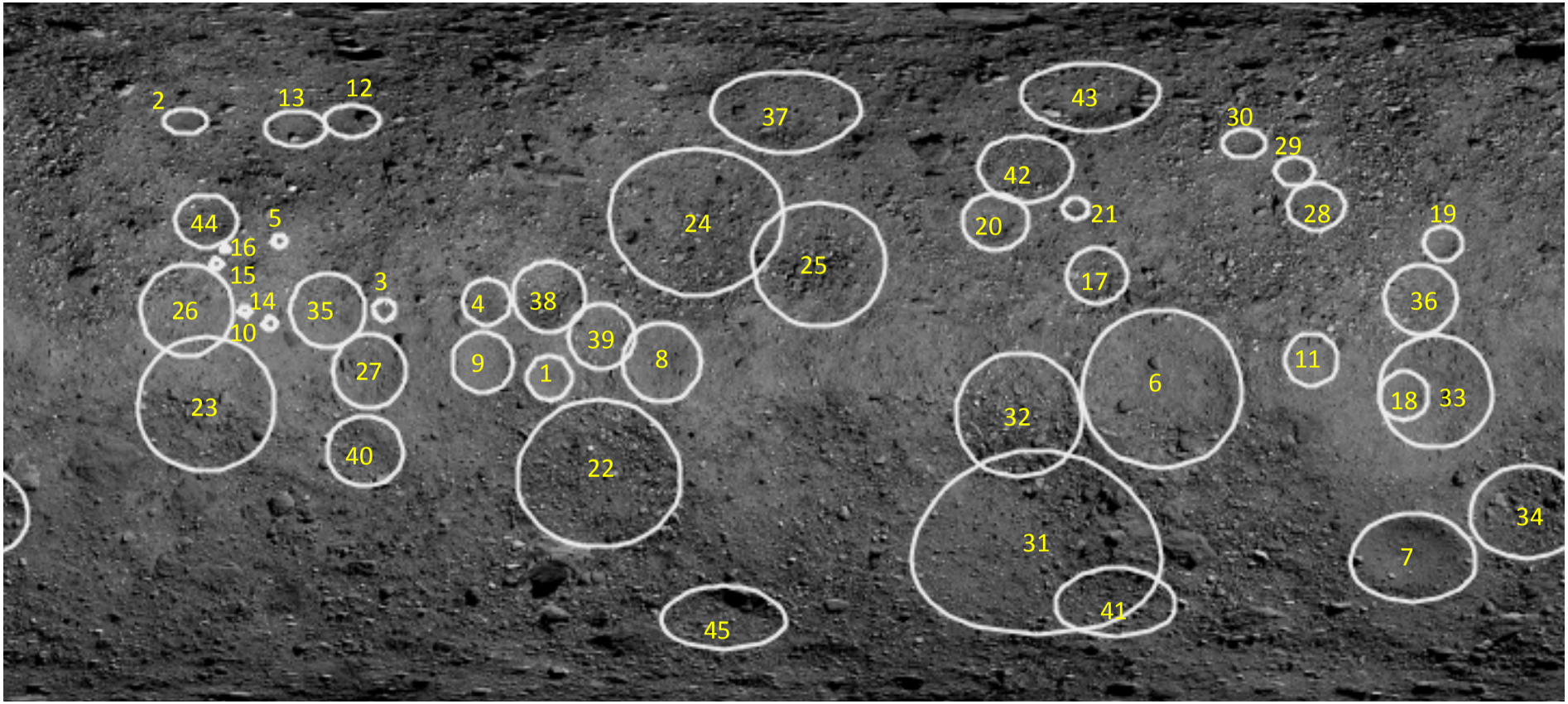

Fig. 1. The craters included in this study are presented here on a global mosaic of Bennu with a pixel scale of 5 cm/pixel (Bennett et al. (2020)). Characteristics of these craters can be found in Table 1 in Appendix A.

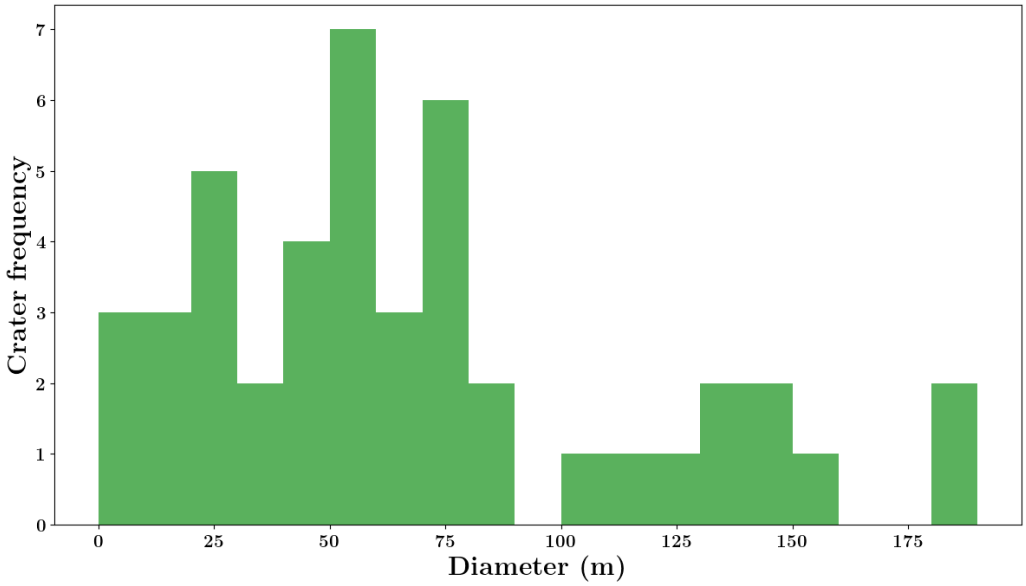

Fig. 2. Frequencies of analyzed craters are displayed as a function of diameter (m), with a binning of 10 m.

3 (EQ3) data set (acquired at $\sim 8°$ of phase angle α from an altitude of $\sim$ 4.8 km on 09 May 2019), which has an almost complete spatial coverage of Bennu (between -80° south to 80° north of latitudes, across all the longitudes), with footprint sizes of $\sim$ 20 m (Lauretta et al. (2017)). We also used the data set of Baseball Diamond Flyby 2, with footprint sizes of $\sim$ 14 m (acquired on 26 September 2019) for analyzing two craters (crater IDs 1 and 5). The photometric correction of these data was performed with a global best-fit McEwen model (Zou et al. (2020)) using the Bennu shape model v20 produced by Barnouin et al. (2019). This shape model has a triangular facet size of $\sim$ 0.8 m; however, the shape model was downgraded to 3 m facet size to better correspond to the typical OVIRS footprint size of 20 m (Zou et al. (2020)).

Other spectral data were sourced from the Reconnaissance (Recon) flybys over four candidate sampling sites at lower altitudes and thus smaller spot sizes. These smaller-spot-size data made it possible to analyze the spectral parameters of the small craters ($<$ 20 m) in our data set. We chose data for 8 craters from Recon A, which were collected at an altitude of $\sim$ 1 km, corresponding to a spot size of $\sim$ 6 m.

The Recon A data sets were photometrically corrected using the Bennu shape model v42 produced by Barnouin et al. (2019) that has a smaller ground sampling ($\sim$ 0.8 m triangular facet size) than the downgraded one used for EQ3, because the footprint sizes were smaller in Recon A. Such a better resolution was required in Recon A to better capture the topographical details needed in accurately calculating geometric parameters (i, e, α angles) for the photometric correction. Finally, the spectra that result from the aforementioned

calibration and correction process, were further monitored to avoid any undesired spectral artifacts due to high detector temperatures or filter segment jumps (Simon et al. (2020)).

2.3 Spectral parameters studied

We defined four spectral parameters for study to gain insight into the physical and compositional properties of Bennu's craters.

1. Minimum position of the band at 2.7 μm

An absorption band near 2.7 μm is attributable to structural OH in phyllosilicates and hence is an indicator of aqueous alteration. Its position and depth can be used to determine OH-bearing phyllosilicate abundance and composition. This minimum band position is thought to be related to the Mg/Fe ratio of the phyllosilicates (Farmer (1974), Beck et al. (2010), Takir et al. (2013)), which depends on the alteration undergone. For average Bennu, Hamilton et al. (2019) determined 2.74±0.01 μm to be the minimum position of this band using disk-integrated spectra. They found analogies between Bennu's spectrum and those of meteorites with petrologic types of CM2.1–2.2, associated with strong aqueous alteration.

We determined the minimum reflectance factor (REFF) value of the spectrum from 2.6 to 3.3 μm. To minimize the effect of channel-to-channel noise, we used a running-box average over three channels, applied before finding the minimum. Because of this method, the uncertainty of the minimum position becomes the sampling separation between two consecutive spectral channels in this spectral range, which is ±5 nm.

2. Depth of the absorption band at 2.7 μm

We chose this spectral parameter to compare the degree of aqueous alteration inside Bennu's craters with global Bennu, where the presence of this band is ubiquitous. OVIRS data at the arrival at Bennu indicated that this band on Bennu occurs at 2.74±0.01 μm (Hamilton et al. (2019)). **If we were to assume identical physical properties of the studied phyllosilicate material (e.g., grain size and porosity), a deeper band would imply more aqueous alteration, while a shallow band would imply either a less aqueous alteration or a dehydration of the phyllosilicate material**. Therefore, an analysis of the band depth of this band makes it possible to infer useful information with regards to aqueous alteration of the material present inside craters.

First, we computed the minimum REFF value (R_{min}) over the wavelength

range of 2.6 to 3.3 μm, which corresponds to the minimum of the absorption band located at 2.7 μm. To account for any channel-to-channel noise, the mean REFF value of the consecutive three channels centered on the minimum position was computed. Similarly, we obtained the REFF of the left (R_{left} at 2.6 μm) and right (R_{right} at 3.3 μm) shoulders of the band by taking the mean REFF of five channels centered at each shoulder wavelength. Then we computed a linear continuum between the two shoulders of the band, which led to an interpolation of the REFF (R_i) value at the minimum position of the band. Then the band depth (BD) was calculated as per Eq. 1.

$$BD = 1 - \frac{R_{min}}{R_i} \tag{1}$$

3. Normalized spectral slope evaluated from 0.55 to 2.0 μm

Spectral slope being a function of both grain size and composition of carbonaceous chondrites, normalized spectral slope is considered in this context, in order to be compatible with literature. We determined the normalized spectral slope from 0.55 to 2.0 μm, respecting the five-channel averaging criteria described above. We computed REFF values at 0.55 μm ($R_{0.55}$) and 2.0 μm ($R_{2.0}$). We calculated the normalized spectral slope (S) according to Eq. 2 and it is expressed in the units of %/0.1 μm.

$$S = \frac{(R_{2.0} - R_{0.55})}{R_{0.55}} \times \frac{10}{2.0 - 0.55} \tag{2}$$

4. Photometrically and thermally corrected reflectance factor at 0.55 μm

In carbonaceous chondrites, the REFF at 0.55 μm (REFF0.55μm) is a function of grain size as well as composition and could depend on surface roughness and observation geometry (without a photometric correction, which is not the case here). We averaged the REFF of the five consecutive channels centered at 0.55 μm. We use this as an estimation of the visible brightness of a given observation.

As shown in Fig. 3, we verified that the original spectral features are preserved in the smoothing process, despite applying a smoothing over three or five channels.

2.4 Preparation of an average spectrum for a crater and an average global spectrum of Bennu for comparison.

Individual spectra available for a given crater were averaged to obtain a single average spectrum, and the aforementioned spectral parameters were computed

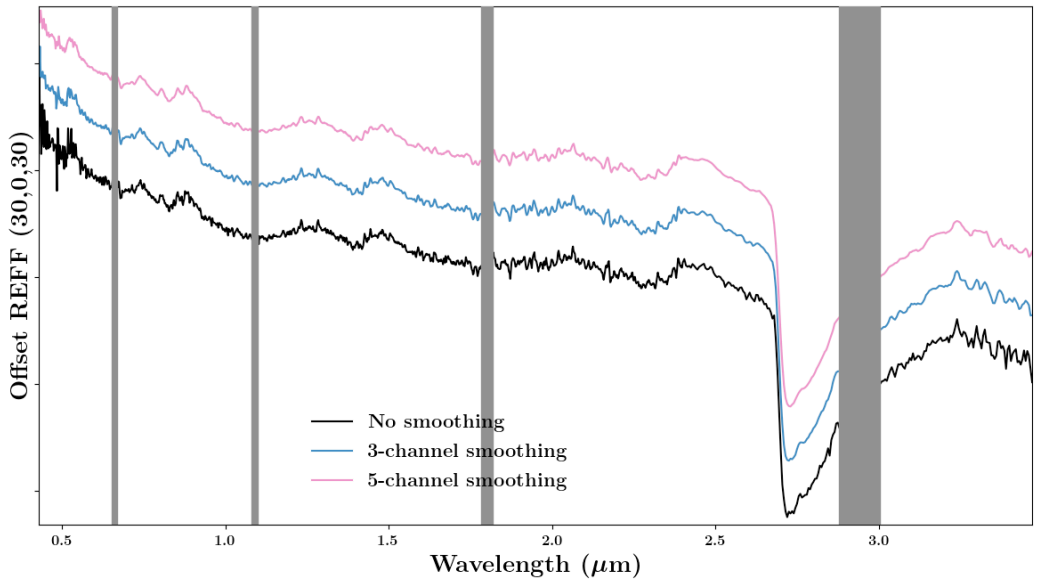

Fig. 3. Average discrete spectrum of crater ID 36 is shown in black, whereas blue and pink spectra correspond to smoothed spectra achieved by a running-box average over three and five spectral channels, respectively. Blue and pink spectra are vertically offset from the black spectrum respectively by 0.001 and 0.002 for clarity. The vertical grey columns represent the wavelengths of the OVIRS filter segment boundaries.

from that average spectrum. This process was repeated for all 45 craters that we studied. Accordingly, the values in Table 1 in Appendix A represent average values for each crater. The uncertainties of each average crater spectrum were computed from the uncertainties of each individual spectrum from that crater. These uncertainties include instrumental, calibration and photometric correction errors.

The average global spectral parameters of Bennu, with which we compared the average spectra of craters, come from the EQ3 data set (acquired at $\sim 8^\circ$ of phase angle α), which provides an almost complete spatial coverage of Bennu. To calculate an average global spectrum of Bennu, we used spectra spread in an equatorial band from -25° to 25° latitudes, excluding spectra with i and e $>40^\circ$. The original viewing geometry of spectra was thus restricted to avoid cases where the photometric correction may not be optimal. This selection resulted in 2775 individual spectra, which we averaged to obtain the average global spectrum of Bennu used in this work.

In Fig. 4, we show an example of an average crater spectrum of crater ID 36, obtained by averaging 26 individual spectra as shown. The average global spectrum of Bennu, calculated as explained above, is also given for comparison. The 2.7-μm band minimum, 2.7-μm band depth, normalized spectral slope and REFF0.55μm of the average global spectrum are 2.735±0.005 μm, 0.1616±0.0001, -0.363±0.003 %/0.1 μm, and 0.02517±0.00001 respectively.

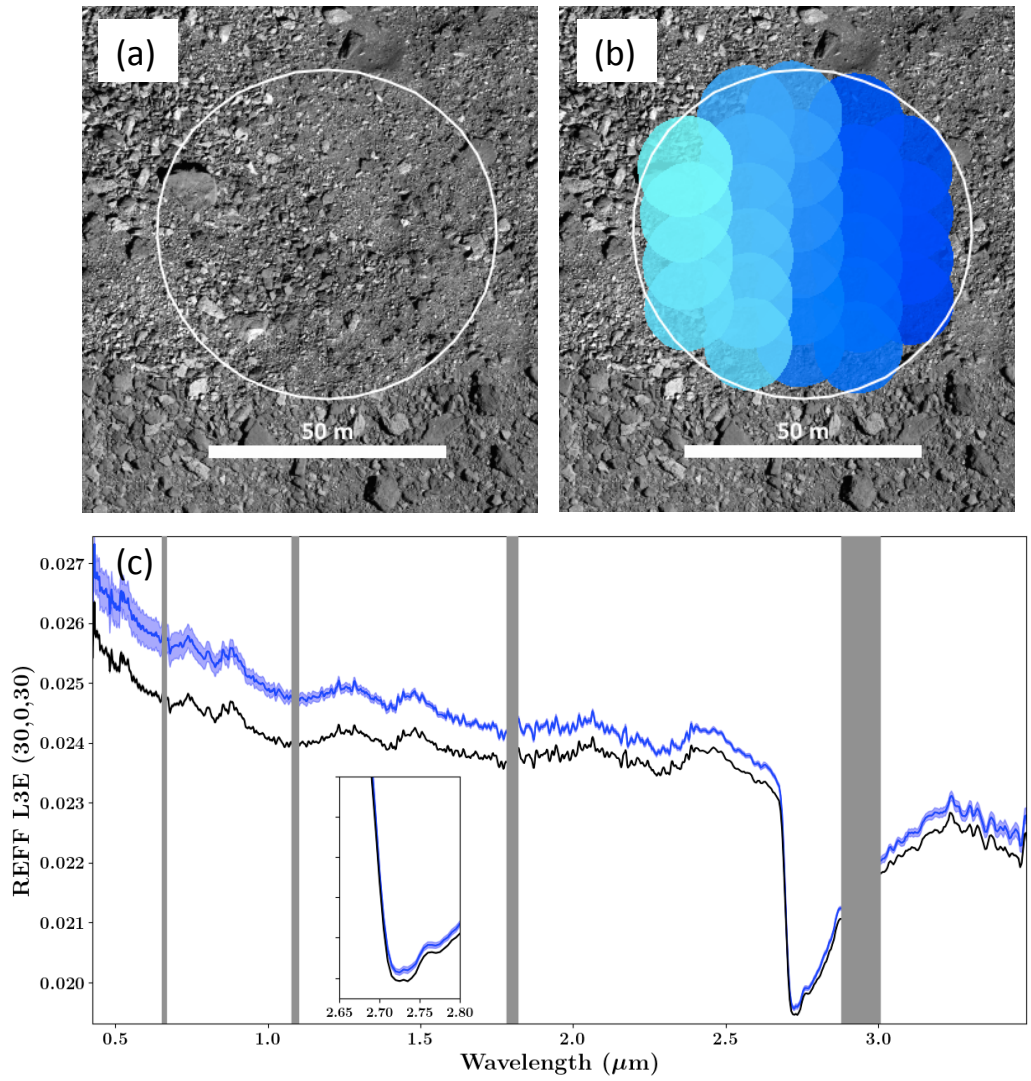

Fig. 4. Panel (a): A view of the crater ID 36. Panel (b) : crater ID 36, with 26 footprints of OVIRS spectra from the EQ3 data set overlain. A gradient of colors is used to distinctively show individual footprints. Panel (c): Average spectrum of this crater (photometrically corrected REFF (i=30°,e=0°,α=30°)) obtained by averaging the 26 spectra, whose footprints are shown in the panel (b) and the global average spectrum of Bennu extracted from the EQ3 data set are shown in blue and black, respectively. The inset shows a zoomed-in view of the minimum position of the 2.7-μm band. Both spectra have been smoothed by a running-box average over three channels and the error-bars represent the uncertainties resulting from the averaging. The error bars on the black spectrum are too small to be visible. The vertical grey columns represent the wavelengths of the OVIRS filter segment boundaries.

Those of the average crater spectrum of crater ID 36 are 2.725±0.005 μm, 0.167±0.001, -0.50±0.03 %/0.1 μm, and 0.0262±0.0001 respectively. Except for the 2.7-μm band minimum, all other parameters have been calculated without a smoothed spectrum, as the channel-to-channel noise is accounted for as described in the section 2.3.

Although we use average spectra of craters to interpret overall spectral trends in the entire data set, we do use individual spectra to highlight some results, depending on their nature.

3 Results

3.1 Shortward shift of the 2.7-μm absorption band

We computed the 2.7-μm absorption band minimum of average crater spectra of the 45 craters, relative to the global Bennu spectrum, that we computed in section 2.4, where the minimum position is at 2.735±0.005 μm (Table 1). We find varying shifts of the 2.7-μm absorption band minimum among the studied craters. We find shortward shifts (δ) of band minima for 20 out of 45 craters. For 20 craters, we find zero shift of the minimum and for the remaining 5 craters, we find longward shifts of the band minima. Fig. 5 shows the variation of the shift in nanometers as a function of crater diameter.

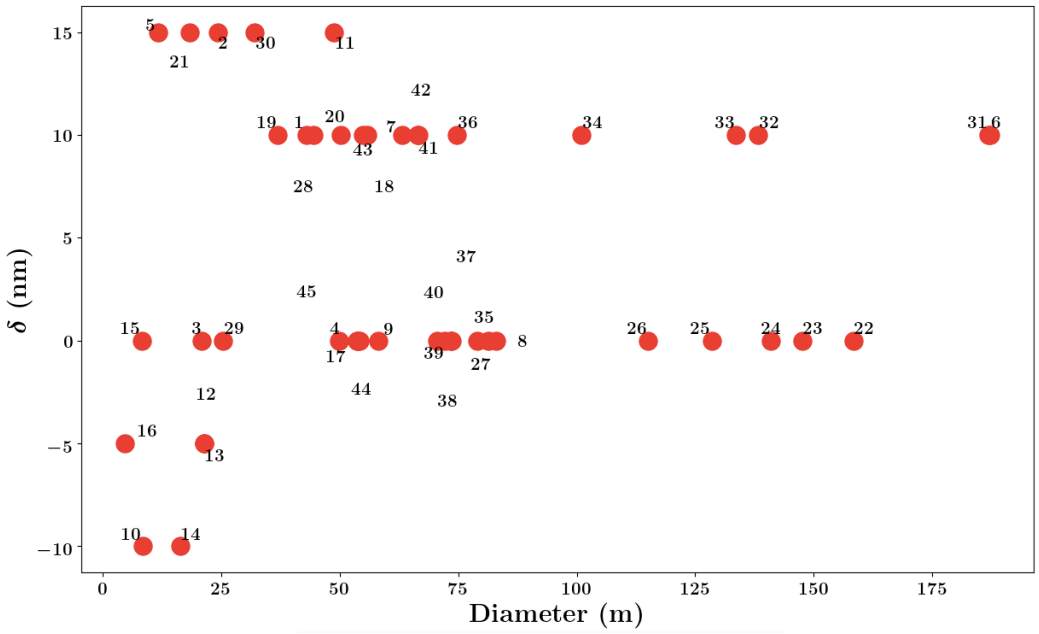

Fig. 5. Shortward shift (δ) of the 2.7-μm absorption band minimum as a function of crater diameter. **For the 45 average crater spectra, the** shift of their 2.7-μm absorption band is measured with respect to 2.735 μm, which is the 2.7-μm band minimum of the global Bennu spectrum, derived from the EQ3 data set. Crater IDs appear in black next to their respective data points.

In examining individual spectra from within craters, we found shortward shifts up to **25 nm in the minimum position of the 2.7-μm absorption band, with respect to a local average spectrum sampled from an area next to the Osprey crater, which is typical of altered material on Bennu**. Fig. 6 shows selected spectra from within Osprey (ID 3) and Nightingale (ID 2) craters, where the shortward shift is evident.

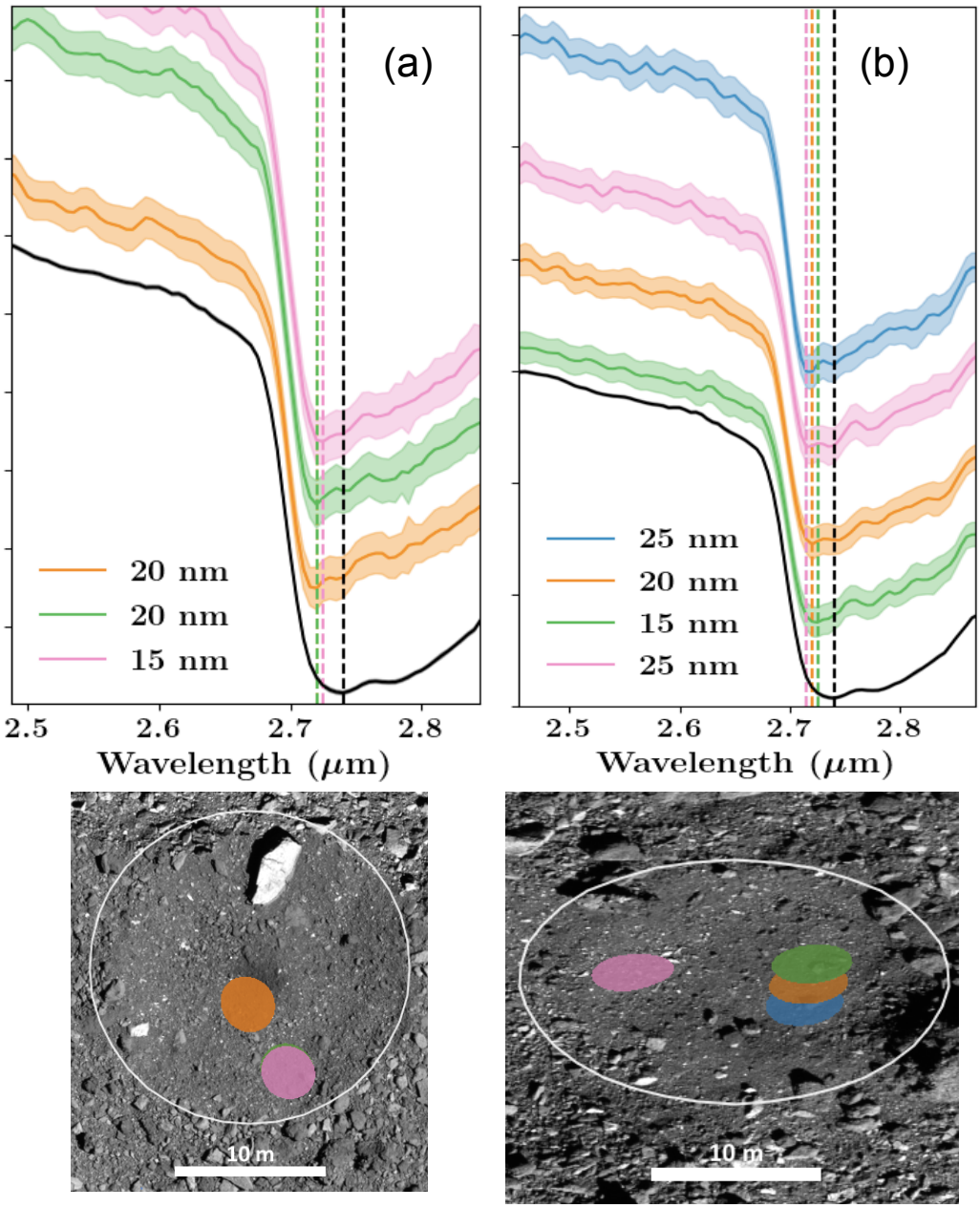

Fig. 6. (a) REFF0.55μm of selected spectra from inside the crater Osprey (ID 3), showing the 2.7-μm absorption band. Spectra are vertically offset for clarity. The dashed vertical lines indicate the minimum position of this band for each spectrum. **A local average spectrum from an area next to the crater is plotted in black, where the 2.7-μm band minimum occurs at 2.74 μm (same as the value detected by Hamilton et al. (2019), Simon et al. (2020)). The shortward shift (δ) of the minimum of the 2.7-μm band, with respect to the latter, for each spectrum is given in the legend**. Below the plots are local maps, where the corresponding OVIRS footprints are projected inside the craters, delimited in white. (b) Same as (a), but for the crater Nightingale (ID 2). These spectra from craters illustrate the shortward shift of the minimum position of the 2.7-μm absorption band and the legends report the corresponding shifts. Nightingale (panel b, ID 2) is the primary sample collection site of the OSIRIS-REx mission, and Osprey (panel a, ID 3) is the back-up site.

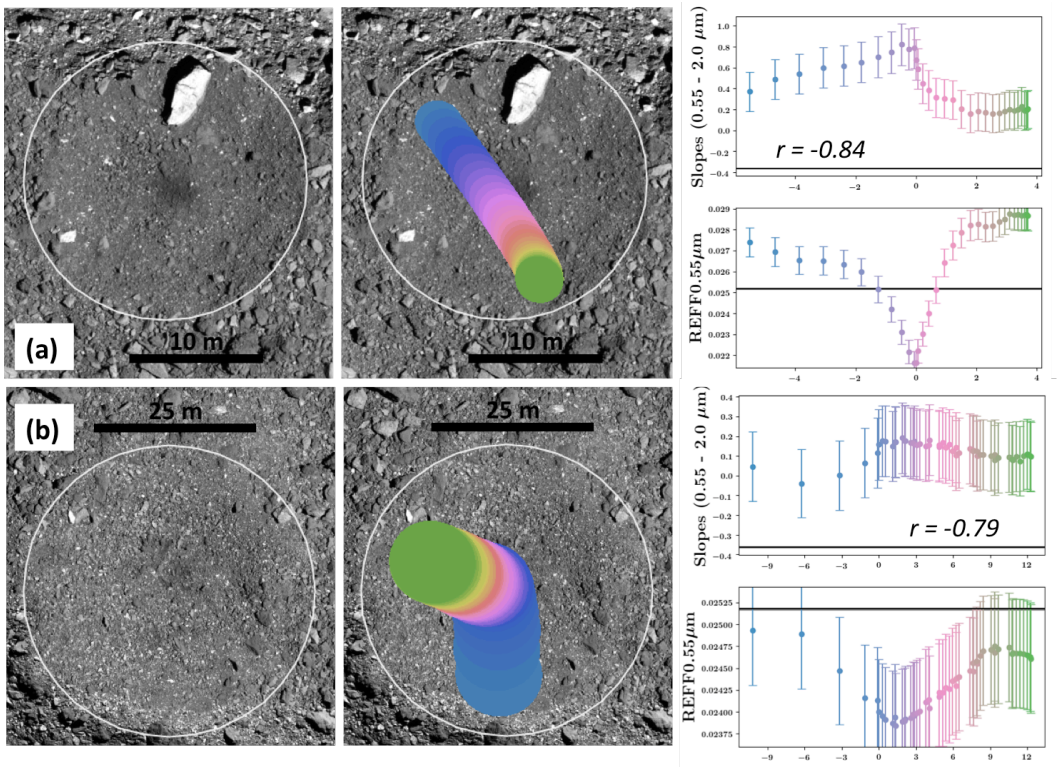

Fig. 7. (a) Osprey (Crater ID 3) without (left) and with (middle) footprints of an OVIRS scan. The rightmost graph shows the spectral slopes and REFF variation as the spectrometer scans across the crater. The x-axis gives the distance (m) to the boresight intercept of a spectrometer footprint, with respect to the footprint that is closest to the centre of the crater during the scan. The distances corresponding to the footprints of spectra acquired prior to the one closest to the centre of the crater are negated. The Pearson coefficient (r) is -0.84 for the relation between REFF0.55μm and spectral slope in this scan, indicating a strong anti-correlation. Corresponding values derived from the global average spectrum are also given for comparison (black horizontal lines with gray uncertainties, which are barely visible). (b) Same as (a), but for crater ID 1. The Pearson coefficient (r) is -0.79 in this case. Error bars are given for the uncertainty of each parameter of an individual spectrum.

3.2 Anti-correlation between spectral slopes and REFF0.55μm

We explored the relation between spectral slopes and REFF0.55μm, two parameters that are widely used to spectroscopically characterize surfaces. We find that their relation varies among craters, and even across different scans of the same crater. We calculated Pearson's correlation coefficient (r) which is a measure of the linear association of two variables (Kirch (2008)). r is restricted to the values in the range [-1, 1]. If the sign of r is positive, it indicates that the two variables increase or decrease together and the two variables are said to be correlated. If r is negative, they are anti-correlated, which indicates that the increase of one variable is associated with the decrease of values of the

other variable and vice versa. The absolute value of r reveals to which extent the two variables are correlated or anti-correlated. The greater the absolute value of r is, the stronger the correlation or the anti-correlation is.

We considered a series of spectra acquired as the spectrometer scanned from the rim of a crater, across its center, and towards the rim again. The REFF0.55μm and spectral slope of each spectrum of this scan were then compared using Pearson's correlation coefficient (r). This process was implemented for all 45 craters in this work. In three cases, an anti-correlation between REFF0.55μm and spectral slope was observed. Fig. 7 shows an anti-correlation between REFF0.55μm and spectral slope (increasing spectral slopes versus decreasing REFF0.55μm) for two of these three craters. This anti-correlation indicates that the spectra become redder and darker closer to the center of the crater.

3.3 Spectral heterogeneity in the largest equatorial crater on Bennu

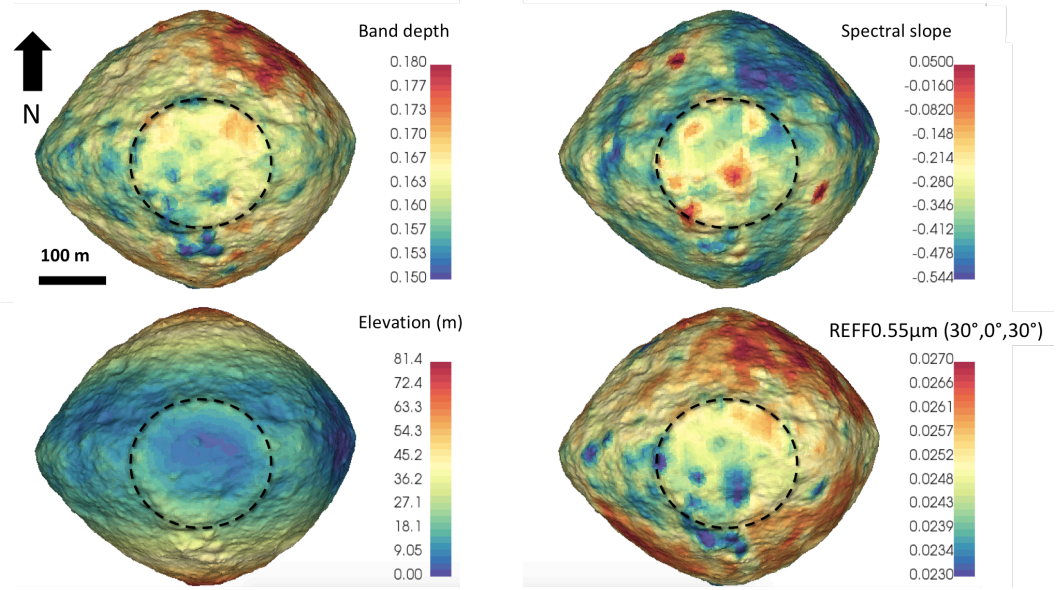

Fig. 8. Representation of 2.7-μm band depth (top left), normalized spectral slope (top right), elevation (bottom left), and REFF0.55μm (bottom right) on a global shape model of Bennu. This shape model contains 196,608 facets, each of which has an edge length of $\sim$ 3 m. The spectral data are mapped to the facets, taking into consideration the facets that were under an OVIRS footprint and computing boresight intercepts at the mid-observation times. The facets that have multiples values were averaged without any weighting. The data are from EQ3, 9 May 2019. The rim of the most prominent crater on Bennu (ID 6) is circled in black.

The equatorial crater (ID 6) centered at -8°, 269° measures 187 m in diameter and is one of the most prominent geological features of Bennu, with a distinguishable raised rim (Walsh et al. (2019)). To investigate possible compositional variation across this large crater, we mapped the spectral parameters

2.7-μm band depth, spectral slope, and REFF0.55μm, as well as elevation, onto a global shape model of Bennu (Fig. 8).

The 2.7-μm band depth varies locally across the crater. When compared to high-latitude band depths, the band depths inside the crater appear to be shallower. The lowest 2.7-μm band depths in the crater are associated with three boulders. The band is shallower in the southern part of the crater than in the north.

The variation of REFF0.55μm across the crater has a similar trend to the 2.7-μm band depth. These two parameters inside this crater are strongly correlated ($r = 0.83$). The lowest REFF0.55μm values (darkest features) inside the crater are associated with the three boulders noted above. Furthermore, the REFF0.55μm results indicate that the crater is darker in the south than in the north.

The trend of spectral slopes inside the crater does not correlate necessarily with the variation in 2.7-μm band depth and REFF0.55μm. Nevertheless, they contribute to the crater's spectral heterogeneity. The reddest spectral slopes are located towards the center of the crater and towards the southwestern rim of the crater.

3.4 Smaller craters appear brighter, with deeper hydration and redder spectral slopes

To explore the relations among spectral slopes, REFF0.55μm, and 2.7-μm band depths of Bennu's craters, we visualized their variations as a function of crater diameter (Fig. 9). The distribution of data points show that the smaller a crater is, the deeper its 2.7-μm band depth is and the brighter it is (Fig. 9, panels b and c). The distribution of spectral slopes in panel (a) of Fig. 9 hints at a similar variation, indicating that smaller craters are spectrally redder, although there seems to be a population of craters with sizes in the range of 20 to 30 m with both spectrally red and blue characteristics. However, the crater frequency distribution with respect to spectral slope, as seen in Fig. 10, implies that 30 craters are spectrally bluer than the mean of the spectral slope of distribution of the 45 craters. Panel (d) of Fig. 9 shows a positive correlation between REFF0.55μm and 2.7-μm band depth, with a few outliers. With the exception of the most distant outlier, which is the Nightingale crater (ID 2), this correlation has a Pearson coefficient (r) of 0.76. This observation implies that, in general, craters with deeper hydration band depths tend to be brighter, and vice versa.

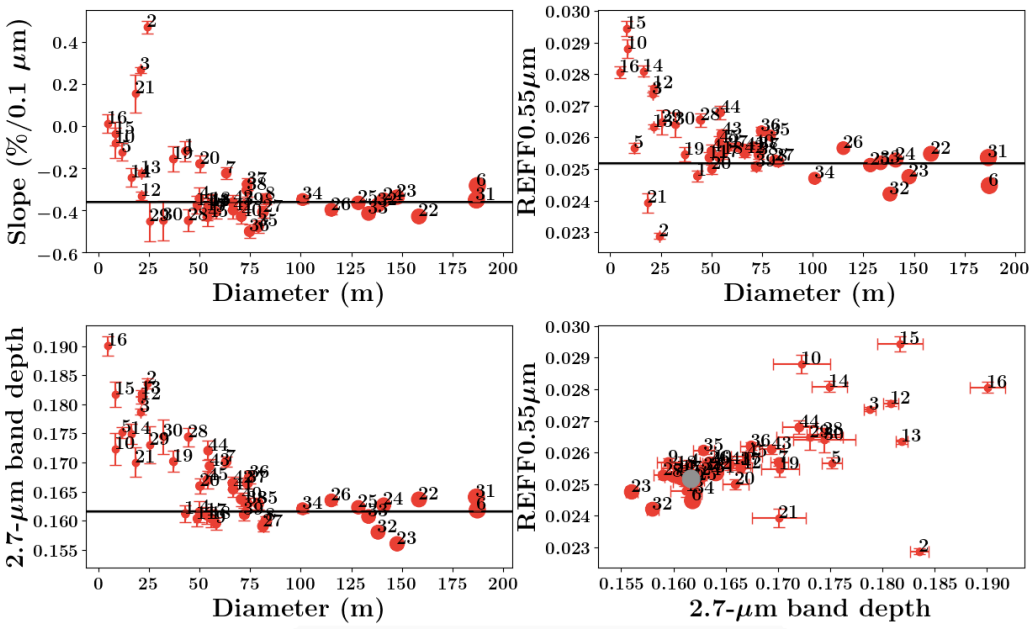

Fig. 9. Variations in (a) normalized spectral slope, (b) REFF0.55μm, and (c) 2.7-μm band depth with crater diameter. The global average values for Bennu, derived from the EQ3 data set, are given as horizontal lines. (d) Variation in REFF0.55μm with 2.7-μm band depth. The global average for Bennu is shown as a gray circle. The sizes of the data points are scaled to corresponding crater diameters, and crater IDs appear in black next to their respective data points. The error bars correspond to propagated uncertainties inherent from calculations.

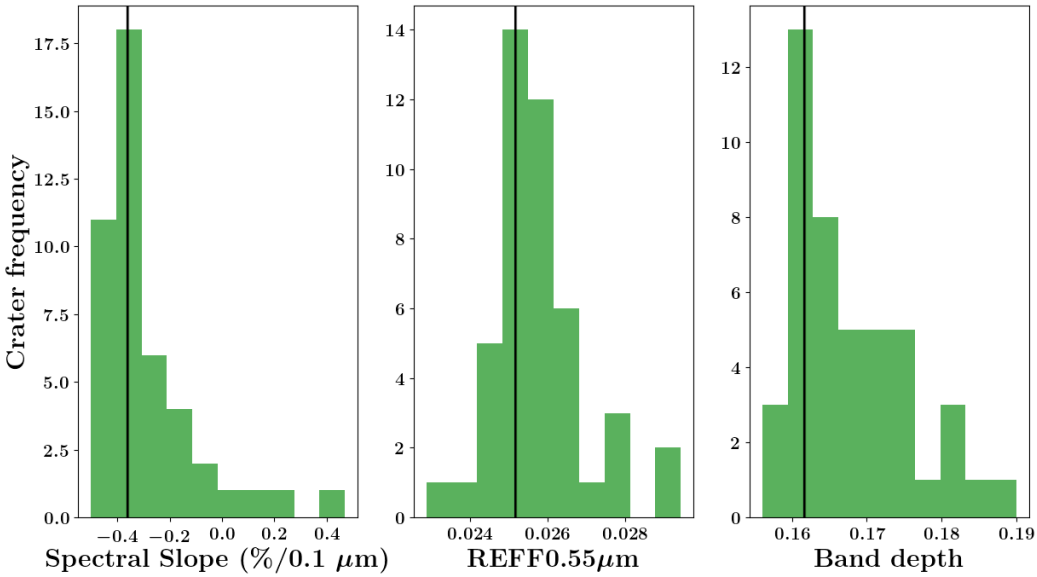

Fig. 10. Crater frequency distribution with respect to spectral slope, REFF0.55μm, and 2.7-μm band depth. The black vertical lines correspond to the global average values for Bennu derived from EQ3 data and their uncertainties, which are too small to be visible.

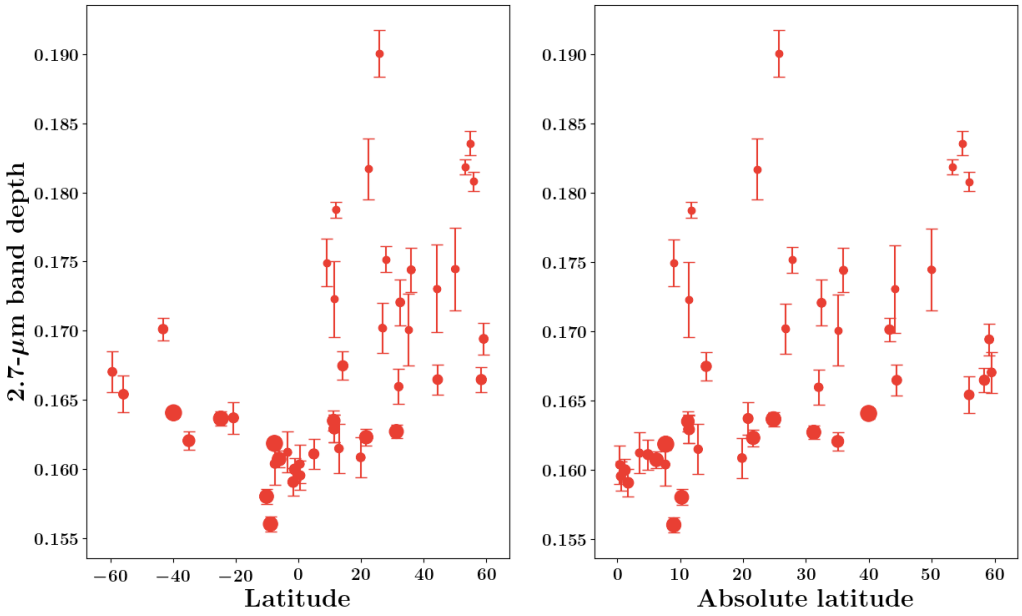

Fig. 11. 2.7-μm band depth of craters as a function of absolute latitude. Data point sizes are scaled to represent the sizes of the craters. The error bars correspond to uncertainties inherent to calculations.

3.5 Weak correlation between 2.7-μm band depth and absolute latitude

When 2.7-μm band depths of craters are plotted as a function of latitude, there appears to be a certain symmetry around the equator as seen in the Fig. (11). However, it can be seen that the data points are insufficient in the southern hemisphere to analyze this trend, as our data do not capture the smaller craters in the southern hemisphere. Nevertheless, it is possible to discern a weak correlation between 2.7-μm band depths and absolute latitude of the craters, whose Pearson's r is 0.49.

4 Discussion

The observed shift of the hydrated phyllosilicate absorption band at 2.7 μm towards shorter wavelengths in craters (Fig 6), relative to the global Bennu spectrum, can be interpreted in several ways. The minimum position of this band in phyllosilicates is an intrinsic function of mineral structure and composition (Takir et al. (2013)). Experimental work has shown that this minimum position can be offset by space weathering (Lantz et al. (2017)), which is the alteration of surfaces of atmosphere-less bodies by physical processes (Hapke (2001)) that include, but are not limited to, sputtering, solar wind irradiation, and meteoroid impacts. Therefore, the observed shortward shifts may be attributed to compositional differences in Mg/Fe ratios in the phyllosilicates or space weathering. We have measured the shifts relative to the minimum at 2.735$\pm$0.005 μm that we derived for global Bennu from the EQ3 data set, which is comparable to the value of 2.74$\pm$0.01 μm that Hamilton et al. (2019) determined for Bennu using disk-integrated spectra. The fact that we observe shortward shifts up to 20 nm in individual spectra implies reliable values above the uncertainties due to spectral sampling, instrumental noise and smoothing of spectra.

Thanks to laboratory experiments simulating solar wind irradiation on carbonaceous chondritic meteorites by Lantz et al. (2017), shifts in the 2.7-μm band can be used to characterize space weathering on C-complex asteroids. The more a surface undergoes space weathering (exposure to space), the more this band shifts towards longer wavelengths. Hence, the shortward shift we report in craters indicates more recently exposed surfaces, as expected. Given that we find these shifts within relatively smaller craters, which are presumably younger, we propose that the observed shortward shifts indicate comparatively short exposure to space weathering. Since craters, and sometimes ejecta surrounding them, are linked to the excavation of subsurface material by the impact event, they should contain more freshly exposed material than the rest of the surface. The crater Nightingale (ID 2), which is the primary sampling site of the mission, exhibits the maximum shift observed (20 nm) for individual spectra, indicating that it contains some of the least exposed, and thus least altered, material (Fig. 6). The samples returned from this crater in 2023 will help establish the ground truth about this.

We reported the shifts of the 2.7-μm band for all the studied craters in Table 1, using their average spectra. As seen in Fig 5, smaller craters appear to have both shortward and longward shifts of this band. However, since largest shortward shifts are found among smaller craters, presumed to be younger, they could contain less altered material. The longward shifts are attributed to compositional differences inside the craters in question.

The other spectral parameters that we examined in this study are not as reliable for characterizing space weathering because their interpretations can be ambiguous in the context of C-complex asteroids. For example, spectroscopic data show both reddening and bluing of spectral slope as consequences of space weathering (Nesvorný et al. (2005), Lantz et al. (2013)). Furthermore, spectral slope also depends on the distribution of particle sizes and porosity of the surface (Cloutis et al. (2018)). The visual brightness is known to decrease or increase, according to laboratory simulations of space weathering on carbonaceous chondrites (Lantz et al. (2017)). Since 2.7-μm band depth is directly linked to the extent of aqueous alteration originally undergone by the material, it cannot be used as a measure of space weathering. Therefore, spectral slope, REFF0.55μm and 2.7-μm band depth are non-unique identifiers of space weathering.

No global trend is apparent between spectral slopes and REFF0.55μm for the craters analyzed. However, within three craters (IDs 1, 3 and 6), the identified anti-correlation between these two parameters among spectrometer scans implies the presence of fine particulates. This interpretation is based on visual inspection (down to cm scale for crater IDs 1 and 6 and to sub-cm scale for crater ID 3; Osprey) of the asteroid's surface under the spectrometer footprints and laboratory experiments on carbonaceous chondrite meteorites that yielded redder spectra for finer grains (Cloutis et al. (2018)). We also observed that the presence of coarser material inside craters modifies the relation between these two parameters. Hence we propose that the relation of REFF0.55μm and spectral slopes of a series of spectra spanning across a crater could be used as a proxy for the presence of fine particulates. Complementarily to this spectral result, morphological analysis of crater interiors (Bierhaus et al. (2019), Bierhaus et al., in preparation) provides supporting evidence for the presence of finer particulates inside craters. The fact that this anti-correlation is observed only for three craters is probably due to mass movement, which introduces coarser material, having affected most of the craters. **It is also noteworthy that Hayabusa2 mission has found similar spectral evidence on the near-Earth asteroid (162173) Ryugu for fine particulates to be present in most of its crater floors (Riu et al. (2020).**

Our spectral investigation of the most prominent, equatorial crater (ID 6, Fig. 8) on Bennu showed that this crater is spectrally heterogeneous, with a pronounced north-to-south dichotomy in 2.7-μm band depth and REFF0.55μm, which are strongly correlated. This dichotomy can be associated to the partial infill of material described by Walsh et al. (2019) and Jawin et al. (2020). This crater may be one of the most primordial surface geological units on Bennu, older than 10 million years, (Walsh et al., 2019), dating back to the asteroid's time in the main belt. Mass movement has deposited material into it, producing the 6-meter-thick infill from its southern side. The reddest spectral slopes, which we interpret to indicate the finest particulate sizes, on the

basis of meteorite spectra and OCAMS images, are found towards the center and southwestern rim of this crater. As such, we propose that spectral heterogeneity inside craters can be used as a tracer for mass movement across an asteroid.

The cause of the observed spectral differences on the surface of this crater can be manifold. The physical parameters such as porosity and particulate dimensions of the material present therein could, on their own or, combined with other physical parameters, mimic a surface that is spectrally heterogeneous. The composition also could play a contributing role in this. For example, the presence of Fe-rich and Mg-rich phyllosilicated could result in shallower and deeper 2.7-μm band depths respectively (Takir et al. (2013)).

The relations among spectral slopes, REFF0.55μm and 2.7-μm band depth as a function of crater diameter show that smaller craters are brighter and have deeper 2.7-μm hydration bands. If we assume that smaller craters on Bennu are younger, this would suggest that the more freshly exposed material in young craters is more hydrated and brighter than the average Bennu terrain. Hence, over time, it would assume darker and less hydrated surface properties, more akin to those of average Bennu. Fig. 10 shows that 28 craters are indeed less hydrated than the mean of the band depth distribution of the 45 craters. (Fig. 10). This finding can be interpreted in the context of the recent Small Carry-on Impactor (SCI) experiment conducted by the Hayabusa2 mission (Arakawa et al. (2017), Kitazato et al. (2020)), which led to creation of an artificial crater with a diameter $\sim$ 15 m on asteroid (162173) Ryugu, another C-complex NEA. Kitazato et al. (2019) reported that 2.7-μm absorption bands in the material inside the SCI crater and its ejecta were deeper than the mean 2.7-μm band on Ryugu. They further found that the spectra of this material showed a shortward shift of the 2.7-μm band minimum, as predicted by laboratory experiments (Lantz et al. (2017)). New near-infrared spectra acquired under vacuum on phyllosilicates confirm the band shift as a result of the ion irradiation (Rubino et al. 2020, submitted). These results from a freshly created crater corroborate our finding that younger craters (comparable in size to the SCI crater) on Bennu have deeper 2.7-μm band depths. Furthermore, the shortward shift of this band discussed earlier fits together with the space weathering scenario, well constrained by the SCI experiment. In light of this, we propose that smaller craters on Bennu contain excavated sub-surface material that is less affected by space weathering and mass movement.

We also found that younger (smaller) craters are spectrally redder. This finding is consistent with the results of DellaGiustina et al. (2020), which were obtained using data from the OCAMS MapCam imager and covered a wider population of craters than those included in our work owing to the better spatial resolution of a MapCam pixel (about 60 times better than an OVIRS footprint). They propose a scenario of space weathering in which craters are

red at their creation, and over time, they evolve to be bluer and converge towards the average colours of Bennu. This model is supported by our observation of a unimodal and skewed distribution of spectral slopes, where we notice the crater frequency peaks at the spectral slope value of average Bennu (Fig. 10). This implies that the redder craters end up becoming bluer and converge towards the value of average Bennu having had the time necessary for space weathering to act on them. Different exposure ages and different weathering rates could be invoked to explain the population of craters in the size range of 20 to 30 m that have both redder and bluer spectra relative to the average (Fig. 9, panel a).

REFF0.55μm and the 2.7-μm band depth are positively correlated, meaning that brighter craters are more hydrated, with a few outliers. It appears that the most distant outlier from this trend, the primary sampling site Nightingale (crater ID 2), appears also at extremes in terms of both spectral slopes and REFF0.55μm among the population of craters studied in our work. As evident from Fig. 9, this crater appears to be the reddest and the darkest of all the studied craters, which makes it spectrally distinct. According to a multivariate statistical analysis of OVIRS data Barucci et al. (2020), this crater is one of the spectrally reddest localized areas on Bennu. We will learn more about the material of this crater from the samples that the mission will return in 2023.

The analysis of the 2.7-μm band minimum position of the crater population (Fig. 5) suggests that crater IDs 2,5,11,21 and 30 contain relatively fresh material given that they have the largest shortward shift (Lantz et al. (2017)) of this band in their average spectra. We checked where these craters plot in the spectral parameter spaces investigated (Fig. 9). The crater IDs 2,5,21 and 30 plot higher than average Bennu in the 2.7-μm band depth space, which means they are more hydrated than average Bennu. In terms of spectral slope, crater IDs 2,5 and 21 plot redder than average Bennu. The REFF0.55μm plot reveals that only crater IDs 5 and 30 are brighter than average Bennu. As for crater ID 11, it has spectral slope, REFF0.55μm and 2.7-μm band depth values similar to those of average Bennu. This comparison, according to the interpretation of global spectral trends of the studied Bennu's craters, allows us to verify, in an independent manner, that the material inside craters IDs 5 and 30 is younger than average Bennu surface. The fact that crater IDs 2,11 and 21 do not perfectly follow the general spectral trend (that younger craters are brighter, more hydrated and spectrally redder) does not necessarily imply a contradiction. As we have seen, there can be outlier craters, that still have shortward shift of the 2.7-μm band minimum position in their average spectra. This is probably due to the limited number of variables in this study, which do not encompass all the physical processes at work on the surface of Bennu.

We also find a weak correlation between 2.7-μm band depths and absolute latitude of the analyzed craters. This relation indicates that the craters located

near the equator are less hydrated than those at higher latitudes. It is possible that this trend is related to mass movement across the asteroid (Jawin et al. (2020)) and its different rates of action depending on latitude. A crater at high latitudes might stay 'fresh' for a longer period of time than one close to the equator or in mid-latitudes, according to the findings of Jawin et al. (2020). However, when looking at REFF0.55μm and spectral slope values of craters, we do not find a strong correlation with the latitude.

5 Conclusions

Our spectral analysis of 45 craters on B-type asteroid Bennu was structured around four spectral parameters from OVIRS data. Based on our findings, we summarize the key take-away messages:

- The shortward shift of the 2.7-μm band inside craters indicates the presence of freshly excavated sub-surface material, which accordingly has undergone less alteration due to space weathering than the average Bennu surface.
- A scan-dependent anti-correlation between REFF0.55μm and spectral slopes is observed for spectra within three craters, with spectra becoming redder and darker towards the center of the given crater. We propose that this anti-correlation is a proxy for the presence of fine particulates inside a crater.
- Spectral heterogeneity inside the most prominent equatorial crater on Bennu (ID 6) implies within-crater physical or compositional differences of the material present. This crater exhibits a partial infilling on its southern side. Accordingly, we propose that spectral heterogeneity of a crater can be used as a tracer of mass movement.
- Younger craters are brighter and have deeper 2.7-μm hydration bands and redder spectral slopes. As they age, they become darker with shallower bands and bluer spectral slopes as a consequence of space weathering processes. The craters presumed to be younger based on the shortward shift of their 2.7-μm band (less space weathered) generally corroborate this spectral trend.
- REFF0.55μm values and the 2.7-μm band depths of craters are positively correlated, meaning that brighter craters are more hydrated.
- Nightingale (Crater ID 2), the primary sample site of the OSIRIS-REx mission, is the reddest and the darkest crater. In the REFF0.55μm and 2.7-μm band depth space, it is the most distant outlier. Nightingale is thus spectrally distinct from the other studied craters.

Although our sample of 45 craters does not capture the entire crater population on Bennu, and its selection was highly subject to the availability of spectral data at favorable spatial scales, the sample spans a large range of crater sizes observed on Bennu. As such, our findings can be considered rep-

resentative of spectral relations among and within craters on a C-complex asteroid. Spectral results from the SCI crater (Tatsumi et al. (2020)) and from natural craters on Ryugu (**Riu et al. (2020), Cho et al. (2020)**, Hirata et al. (2020)) could aid further interpretation of the trends we report for Bennu and impose additional constraints on a more global scale. Finally, the eventual return to Earth of samples from both Ryugu and Bennu, expected respectively in late 2020 and late 2023, will provide ground truth about the surface properties of C-complex NEAs, furthering the know-how of interpreting remote-sensing data collected from robotic space missions.

Acknowledgements

We extend our grateful thanks to the teams at University of Arizona, NASA and Lockheed Martin for the hitherto achieved success of the OSIRIS-REx mission and wish all the best for the remainder of the mission. This material is based on work supported by NASA under Contract NNM10AA11C issued through the New Frontiers Program. JDPD, MAB, AP, PHH, SF, FM, MF and CL acknowledge funding support from CNES. JDPD extends his thanks to kind friends at Fondation Marjolin for their support. PHH acknowledges funding support by the DIM ACAV+ program of the Region Ile-de-France. EAC thanks the Canadian Space Agency, NSERC, CFI, MRIF, and UWinnipeg for supporting this study. JRB and GP were supported by Italian Space Agency grant agreement n. 2017-37-H.0.

6 Data Availability

OVIRS data from Equatorial Station 3 and Recon A are available via the Planetary Data System at https://sbn.psi.edu/pds/resource/orex/ovirs.html. Data are delivered to the PDS according to the OSIRIS-REx Data Management Plan available at https://sbn.psi.edu/pds/resource/orex/orexmission.html. Shape models will be available in the PDS 1 year after departure from the asteroid. SBMT and select shape models of Bennu are available via https://sbmt.jhuapl.edu

References

Acton, C., Bachman, N., Semenov, B., & Wright, E. 2018, Planetary and Space Science, 150, 9

Acton, C. H. 1996, Planetary and Space Science, Volume 44, Issue 1, p. 65-70., 44, 65

Annex, A., Pearson, B., Seignovert, B., et al. 2020, Journal of Open Source Software, 5
Arakawa, M., Wada, K., Saiki, T., et al. 2017, Space Science Reviews, 208, 187
Barnouin, O. S., Daly, M. G., Palmer, E. E., et al. 2019, Nature Geoscience, 12, 247
—. 2020, Planetary and Space Science, 180, 104764
Barucci, M. A., Hasselmann, P. H., Praet, A., et al. 2020, AA, 637, L4
Beck, P., Quirico, E., Montes-Hernandez, G., et al. 2010, Geochimica et Cosmochimica Acta, 74, 4881
Bennett, C. A., DellaGiustina, D. N., Becker, K. J., et al. 2020, Icarus, 113690
Bierhaus, E., Barnouin, O., Walsh, K., et al. 2019, in , EPSC–DPS2019–1134
Bierhaus, E. B., McEwen, A. S., Robbins, S. J., et al. 2018, Meteorit Planet Sci, 53, 638
Bottke, W. F., Vokrouhlický, D., Ballouz, R.-L., et al. 2020, The Astronomical Journal, 160, 14
Cho, Y., Morota, T., Kanamaru, M., et al. 2019 (EGU General Assembly), 7032
Cho, Y., Morota, Y. T., Kanamaru, M., et al. 2020, Journal of Geophysical Research (in revision)
Clark, B. E., Binzel, R. P., Howell, E. S., et al. 2011, Icarus, 216, 462
Cloutis, E. A., Pietrasz, V. B., Kiddell, C., et al. 2018, Icarus, 305, 203
Daly, M. G., Barnouin, O. S., Dickinson, C., et al. 2017, Space Science Reviews, 212, 899
Daly, M. G., Barnouin, O. S., Seabrook, J. A., et al. 2020, Sci Adv, 6, eabd3649
DellaGiustina, D. N., Emery, J. P., Golish, D. R., et al. 2019, Nature Astronomy, 3, 341
DellaGiustina, D. N., Burke, K. N., Walsh, K. J., et al. 2020, Science, eabc3660
DeMeo, F. E., Binzel, R. P., Slivan, S. M., & Bus, S. J. 2009, Icarus, 202, 160
Ernst, C. M., Barnouin, O. S., Daly, R. T., & SBMT-Team. 2018 (Lunar and Planetary Science Conference 49), abstr. 1043
Farmer, V. C. 1974, in The Infrared Spectra of Minerals (Mineralogical Society of Great Britain and Ireland)
Fassett, C. I. 2016, J. Geophys. Res. Planets, 121, 1900
Galiano, A., Palomba, E., Longobardo, A., et al. 2019, Icarus, 318, 75
Hamilton, V. E., Simon, A. A., Christensen, P. R., et al. 2019, Nature Astronomy, 3, 332
Hapke, B. 2001, Journal of Geophysical Research, 106, 10039
Hirata, N., Morota, T., Cho, Y., et al. 2020, Icarus, 338, 113527
Jawin, E. R., Walsh, K. J., Barnouin, O. S., et al. 2020, J. Geophys. Res. Planets, 125, e2020JE006475
Kirch, W. 2008, in Encyclopedia of Public Health, ed. W. Kirch (Dordrecht: Springer Netherlands), 1090–1091
Kitazato, K., Milliken, R. E., & Iwata, T. 2020, Science (in revision)
Kitazato, K., Milliken, R. E., Iwata, T., et al. 2019, in (Asteroid science in the

age of Hayabusa2 and OSIRIS-REx), abstr. 2106
Lantz, C., Brunetto, R., Barucci, M., et al. 2017, Icarus, 285, 43
Lantz, C., Clark, B. E., Barucci, M. A., & Lauretta, D. S. 2013, Astronomy and Astrophysics, 554, A138
Lauretta, D., E., B. A., A., B. M., et al. 2015, Meteorit Planet Sci, 50, 834
Lauretta, D. S., Balram-Knutson, S. S., Beshore, E., et al. 2017, Space Science Reviews, 212, 925
Longobardo, A., Palomba, E., Carrozzo, F., et al. 2019, Icarus, 318, 205
Melosh, H. J. 1989, Impact cratering : a geologic process (AA(Arizona, University, Tucson, AZ): New York : Oxford University Press ; Oxford : Clarendon Press)
Musy, M., Jacquenot, G., Dalmasso, G., et al. 2019, "vtkplotter, a python module for scientific visualization and analysis of 3D objects and point clouds based on VTK (Visualization Toolkit), , , doi:http://doi.org/10.5281/zenodo.2561402
Nesvorný, D., Jedicke, R., Whiteley, R. J., & Ivezić, 2005, Icarus, 173, 132
Reuter, D. C., Simon, A. A., Hair, J., et al. 2018, Space Science Reviews, 214, 54
Riu, L., Pilorget, C., Milliken, R., et al. 2020, Icarus (in revision)
Rizk, B., Drouet d'Aubigny, C., Golish, D., et al. 2018, Space Science Reviews, 214, 26
Robbins, S. J., Watters, W. A., Chappelow, J. E., et al. 2018, Meteorit Planet Sci, 53, 583
Scheeres, D. J. 2012, Orbital Motion in Strongly Perturbed Environments (Springer, Berlin, Heidelberg), doi:https://doi.org/10.1007/978-3-642-03256-1
Scheeres, D. J., McMahon, J. W., French, A. S., et al. 2019, Nature Astronomy, 3, 352
Scheeres, D. J., McMahon, J. W., Brack, D. N., et al. 2020, J. Geophys. Res. Planets, 125, e2019JE006284
Simon, A., Reuter, D., Gorius, N., et al. 2018, Remote Sensing, 10, 1486
Simon, A. A., Kaplan, H. H., Hamilton, V. E., et al. 2020, Science, eabc3522
Strom, R. G., Malhotra, R., Ito, T., Yoshida, F., & Kring, D. A. 2005, Science, 309, 1847
Takir, D., Emery, J. P., Mcsween Jr., H. Y., et al. 2013, Meteorit Planet Sci, 48, 1618
Tatsumi, E., Honda, R., Yamada, M., et al. 2020 (Lunar and Planetary Science Conference), 1128
Thomas, P. C. 1993, Icarus, 105, 326
Walsh, K. J., Jawin, E. R., Ballouz, R. L., et al. 2019, Nature Geoscience, 12, 242
Zou, X.-D., Li, J.-Y., Clark, B. E., et al. 2020, Icarus, 114183

Appendix A

Table 1: Characteristics of the analyzed craters. The spectral parameters are derived from the average spectrum of a crater, obtained by averaging multiple spectra, as described in the text. 'Lat.', 'Long.', and 'D' refer to latitude, longitude, and diameter, respectively, from Bierhaus et al., 2020 (in preparation).'Data' refers to the OSIRIS-REx observation during which the data were acquired (Lauretta et al. (2017)). EQ3 refers to Equatorial Station 3 (9 May 2019). B2R is the re-fly of Baseball Diamond Flyby 2 (26 September 2019; originally flown as part of the Detailed Survey mission phase in spring 2019, repeated owing to a communication outage on the first attempt). RA refers to Recon A flybys over the final four candidate sampling sites (weekly in October 2019): Sandpiper (S), Osprey (O), Kingfisher (K), and Nightingale (N). δ is the shift in nm of the minimum position of the 2.7-μm band, measured shortward relative to 2.735 μm. A negative value indicates a longward shift relative to 2.735 μm. Normalized spectral slope (S) is given in units of (%/0.1 μm).

ID	Lat. (°)	Long. (°)	D (m)	Data	δ	N°	2.7-μm band depth	S	REFF0.55μm
1	-3.5	125.9	43.1	EQ3	10	13	0.1612±0.0015	-0.120±0.048	0.02478±0.00017
2	54.9	41.7	24.4	RAN	15	41	0.1836±0.0009	0.470±0.029	0.02288±0.00009
3	11.8	88.1	20.9	RAO	0	147	0.1788±0.0006	0.266±0.015	0.02737±0.00006
4	12.9	111.3	49.9	EQ3	0	10	0.1615±0.0018	-0.346±0.053	0.02557±0.00020
5	27.8	63.7	11.8	B2R	15	16	0.1752±0.0009	-0.123±0.043	0.02567±0.00016
6	-7.7	269.2	187.2	EQ3	10	171	0.1618±0.0004	-0.284±0.013	0.02448±0.00005
7	-43.3	325.2	63.2	EQ3	10	38	0.1701±0.0008	-0.225±0.028	0.02569±0.00010
8	-1.2	152.6	82.9	EQ3	0	46	0.1600±0.0008	-0.348±0.025	0.02523±0.00009
9	0.6	114.1	58.2	EQ3	0	28	0.1595±0.0011	-0.408±0.031	0.02569±0.00012
10	11.4	55.7	8.5	RAK	-10	6	0.1723±0.0027	-0.080±0.072	0.02880±0.00030
11	0.4	302.2	48.9	EQ3	15	15	0.1604±0.0014	-0.376±0.043	0.02536±0.00016
12	56.0	77.5	21.5	RAN	-5	68	0.1808±0.0007	-0.334±0.020	0.02756±0.00008

13	53.3	68.1	21.5	RAN	-5	116	0.1819±0.0005	-0.223±0.016	0.02634±0.00006
14	9.0	61.3	16.4	RAK	-10	16	0.1749±0.0017	-0.245±0.042	0.02809±0.00018
15	22.3	48.9	8.3	RAK	0	10	0.1817±0.0022	-0.036±0.056	0.02944±0.00024
16	25.7	50.8	4.7	RAK	-5	16	0.1900±0.0016	0.011±0.044	0.02805±0.00017
17	19.8	252.6	53.7	EQ3	0	14	0.1608±0.0014	-0.403±0.044	0.02537±0.00017
18	-7.7	324.7	55.8	EQ3	10	13	0.1604±0.0015	-0.373±0.046	0.02549±0.00018
19	26.8	333.3	37.0	EQ3	10	8	0.1702±0.0018	-0.157±0.061	0.02546±0.00023
20	32.0	229.8	50.2	EQ3	10	17	0.1659±0.0013	-0.180±0.041	0.02499±0.00015
21	35.1	248.0	18.5	EQ3	15	4	0.1701±0.0026	0.154±0.090	0.02393±0.00030
22	-24.8	136.9	158.4	EQ3	0	109	0.1636±0.0005	-0.431±0.016	0.02548±0.00006
23	-9.0	46.5	147.6	EQ3	0	113	0.1560±0.0006	-0.339±0.016	0.02475±0.00006
24	31.3	161.2	141.0	EQ3	0	123	0.1627±0.0005	-0.353±0.015	0.02528±0.00006
25	21.6	189.2	128.4	EQ3	0	91	0.1623±0.0006	-0.366±0.017	0.02512±0.00007
26	11.2	41.8	115.1	EQ3	0	56	0.1635±0.0007	-0.399±0.022	0.02566±0.00009
27	-1.7	84.4	81.3	EQ3	0	34	0.1590±0.0010	-0.410±0.028	0.02527±0.00011
28	36.0	303.6	44.5	EQ3	10	10	0.1744±0.0016	-0.451±0.052	0.02655±0.00021
29	44.1	298.6	25.5	EQ3	0	3	0.1730±0.0032	-0.455±0.095	0.02648±0.00038
30	49.9	287	32.0	EQ3	15	3	0.1744±0.0030	-0.451±0.095	0.02640±0.00038
31	-40.0	238.1	186.7	EQ3	10	176	0.1640±0.0004	-0.353±0.013	0.02536±0.00005
32	-10.2	234.1	138.2	EQ3	10	99	0.1580±0.0006	-0.376±0.017	0.02421±0.00006
33	-6.2	333.0	133.5	EQ3	10	83	0.1607±0.0006	-0.417±0.018	0.02519±0.00007
34	-35.1	352.0	101.0	EQ3	10	68	0.1620±0.0007	-0.351±0.020	0.02470±0.00008
35	11.4	74.5	79	EQ3	0	31	0.1629±0.0010	-0.479±0.029	0.02606±0.00012
36	14.1	328.0	74.7	EQ3	10	26	0.1675±0.0010	-0.502±0.032	0.02620±0.00013
37	58.4	181.5	73.6	EQ3	0	34	0.1665±0.0009	-0.278±0.029	0.02562±0.00011
38	11.4	122.6	73.5	EQ3	0	28	0.1629±0.0010	-0.305±0.032	0.02545±0.00012
39	4.9	136.9	72.2	EQ3	0	25	0.1611±0.0011	-0.378±0.033	0.02508±0.00013
40	-20.8	83.9	70.7	EQ3	0	24	0.1637±0.0011	-0.431±0.034	0.02569±0.00013
41	-56.0	256.0	66.6	EQ3	10	16	0.1654±0.0013	-0.401±0.041	0.02562±0.00016

42	44.5	237.5	66.5	EQ3	10	23	0.1665±0.0011	-0.365±0.035	0.02551±0.00013
43	59.3	252.4	55.0	EQ3	10	20	0.1694±0.0012	-0.381±0.037	0.02610±0.00015
44	32.5	47.0	54.3	EQ3	0	10	0.1720±0.0017	-0.381±0.052	0.02679±0.00021
45	-59.5	165.6	53.9	EQ3	0	14	0.1670±0.0015	-0.433±0.044	0.02586±0.00017